Novel Noise Reduction Methods

Samu Taulu, Juha Simola, Jukka Nenonen and Lauri Parkkonen

Abstract Magnetoencephalography (MEG) is a non-invasive neuroimaging tool that offers a combination of excellent temporal and good spatial resolution, provided that the acquired signals have a high enough signal-to-noise ratio. This requirement is often compromised as MEG signals are very weak and often masked by interfering signals from environmental noise sources present at most MEG sites. Even more challenging interference is encountered if the subject carries any magnetic material attached to the body, which is sometimes inevitable in clinical settings, e.g., due to therapeutic stimulators. Therefore, to enable reliable data analysis, it is very important to reduce the contribution of noise in MEG signals as efficiently as possible. In this chapter, we review the basic characteristics of MEG signals, give a short review on traditional approaches to suppress noise, and describe some examples of modern noise reduction methods. Specifically, we emphasize the usefulness of advanced mathematical algorithms applied on the multichannel MEG data.

Keywords Noise suppression · Signal processing · Magnetic shielding · Signal space · Multichannel measurement · Interference · Calibration accuracy · Crosstalk · Signal space projection · Signal space separation · Active compensation · Principal component analysis · Independent component analysis · Spatial filtering · Artifact

S. Taulu (✉) · J. Simola · J. Nenonen · L. Parkkonen
Elekta Oy, P.O. Box 34, 00531 Helsinki, Finland
e-mail: Samu.Taulu@elekta.com

L. Parkkonen
Department of Biomedical Engineering and Computational Science, Aalto University School of Science, Espoo, Finland

S. Supek and C. J. Aine (eds.), *Magnetoencephalography*,
DOI: 10.1007/978-3-642-33045-2_2, © Springer-Verlag Berlin Heidelberg 2014

1 Introduction to Noise Reduction

1.1 Characteristics of MEG Signals and Interference

In MEG, we make inferences about neural processes based on the magnetic field produced by the associated neural currents (see, e.g., Hämäläinen et al. 1993). This magnetic field is detected outside of the head with sensors that are sensitive enough to capture those very weak signals, typically on the order of 10–1,000 fT at the usual measurement distance from the brain tissue. To date, the only technically practical and sufficiently sensitive sensor for MEG is the superconducting quantum interference device (SQUID) (see, e.g., Wikswo 2004; Clarke and Braginski 2006) although other potentially promising sensor types have also been introduced, such as atomic, or optical, magnetometers (Kominis et al. 2003) and GMR-based "mixed sensors" (Pannetier et al. 2004). Regardless of the sensor type, estimation of the neural sources underlying the MEG signals is compromised by inaccuracies posed by the MEG hardware itself and, more importantly, by magnetic interference from sources external to the brain. Due to the weakness of the brain signals, interference quite often dominates the measured MEG data and should therefore be identified and suppressed as accurately as possible. Thus, it is important to model the interference in MEG data even more precisely than the brain signal contribution. When successful, this modeling enables accurate extraction and suppression of the interference and thus facilitates reliable source analysis. However, it is quite common that source reconstruction algorithms are applied on acquired signals with the assumption of ideal hardware and ideal measurement conditions. If these assumptions were true, then one could directly fit forward models derived from Maxwell's equations to the measured data, and find the most plausible source configuration among all possible source distributions. This inverse problem, which inherently does not have a unique solution (Helmholtz 1853), only requires information about the source geometry with respect to the detected magnetic field. Yet, to obtain most accurate and reliable results, the compliance of the recorded signals with Maxwell's equations must be verified. Furthermore, the contribution of magnetic signals from sources outside of the brain should be suppressed.

Before we discuss the different types of interference that can distort the MEG signal and the approaches that can be used to suppress them, let us first review some of the basic concepts and characteristics of MEG signals. Each SQUID sensor is coupled to a pick-up loop that measures the flux of the magnetic induction field $\mathbf{B}$ through the loop. Specifically, the flux can be expressed as the surface integral of the field $\mathbf{B}$ over the area of the pick-up loop: $\phi = \int \mathbf{B} \cdot \mathbf{ds}$.

The first MEG measurements were performed with only one sensor (Cohen 1968, 1972). The number of sensors simultaneously detecting the flux at distinct locations was small until the 1980s when the size of the sensor array started to grow rapidly. Today, modern MEG systems contain hundreds of sensors (e.g. Clarke and Braginski 2006, Chap. 11). The multichannel output of these systems can be expressed as a time-varying vector in the *signal space*, a concept introduced

in the 1980s (Ilmoniemi 1981; Ilmoniemi and Williamson 1987; Ilmoniemi et al. 1987). Sampling theory (Ahonen et al. 1993) is crucial for the design of sensor arrays as well as for understanding the physical aspects of the multichannel signals, especially their spatial complexity and information content.

Various system issues in multichannel MEG systems complicate the interference suppression and signal analysis (Clarke and Braginski 2006, Chap. 7). Sensors packed close to each other in a multichannel array always suffer from crosstalk phenomena to some extent. These couplings, of the order of 1 %, typically arise from inductive coupling between the pick-up coils and feedback currents of the neighbouring MEG channels. Such cross-talk between the channels distorts the signals even in the absence of any external interference or hardware calibration errors. Therefore, cross-talk should be computationally or experimentally determined and compensated for to get an estimate of the cross-talk-free signal. Alternatively, the signals could be compensated for cross-talk in the forward model. Another major concern possibly violating our assumption of the direct applicability of Maxwell's equations on measured signals are the calibration errors. For example, the electronic components used to transform the actual magnetic flux to a voltage may contain gain errors distorting the measurement. Manufacturing of the sensors is not infinitely accurate; there may be slight variations in the surface areas of the pick-up loops, locations and orientations of the sensor may deviate from the nominal ones, and the gradiometers may exhibit small imbalances. Therefore, it is important to calibrate the system as accurately as possible before estimating any source parameters from the data with mathematical models.

In this chapter, we concentrate on interference suppression methods operating at the sensor level of a multichannel MEG system. We do not assume any specific neural source model although some source modeling approaches, such as the beamformer, may also efficiently suppress interfering signals. We will mainly describe approaches for processing of the sensor-level data that can subsequently be used for analysis with any desired source modeling method. Regarding nomenclature, although "noise" is a commonly used general term to describe all kinds of magnetic disturbance fields and artifacts, we prefer to classify different types of MEG disturbance as follows: our use of "interference" will refer to non-physiological sources that are clearly unrelated to the MEG sensor array whereas our use of "noise" will refer to sensor or radiation-shield noise caused by random processes.

1.2 Sampling of the Neuromagnetic Field

All interference suppression methods make assumptions about the separability and detectability of interference and signals of interest. Such assumptions may include *a priori* information about the spatial, temporal, or spectral features characteristic to the different signal components. One of the fundamental questions is whether

we can decompose the multichannel measurements into unique subsets of basic components, some containing only interference and others only neural signals.

In the spatial domain, the number of degrees of freedom, or the effective rank of the neuromagnetic data, has been extensively studied in the past (Ahonen et al. 1993). This spatial sampling theory for MEG is based on the fact that a multichannel MEG measurement can be considered as spatial sampling of the continuous neuromagnetic field. The theory shows that the measurable MEG signals are limited to the low end of the spatial-frequency spectrum. As a practical consequence, there is an upper limit to the number of sensors and a lower limit to the minimum distance between adjacent sensors. Specifically, it has been shown that for MEG signals measured at the minimum distance d, the contribution of spatial frequencies higher than $1/(2d)$ is below the sensor noise and therefore insignificant. Thus, the part containing biomagnetic information in the measured signals is limited in spatial complexity, which also means that the number of degrees of freedom of MEG data is limited. Although this reduces the effective rank of the data to about 100, hundreds of MEG channels are needed to reliably estimate the basis components spanning all detectable signals (e.g. Nenonen et al. 2004; Taulu and Kajola 2005).

1.3 Challenges Specific to MEG

The basic challenge of MEG stems from the fact that the neural currents are weak and aligned coherently in the brain only over a short distance, and the associated magnetic field is measured by sensors outside of the head. Additionally, with SQUID-based detectors, the sensor-to-source distance is further increased by the necessary thermal insulation layer of the helium dewar, about 20 mm. Consequently, the amplitude of the neuromagnetic signal detected in MEG is in the range from 10 to 1,000 fT.

The weakness of the signal can be overcome by increasing the sensitivity of the sensors; however, sensors that are more sensitive are also more susceptible to ambient interference fields, which may eventually exceed the dynamic range of the sensors. Clinical environments are often magnetically noisy, with a variety of electrical equipment radiating magnetic interference not only at the power line frequency and its harmonics, but also across a wide frequency range reaching from near DC up to several GHz. Interference at the lower end of the frequency range is usually due to traffic (cars, trains, trams) and large moving objects inside the building (e.g. elevators). The typical low-frequency peak-to-peak variation of the magnetic field in such an environment is a couple of μT.

To measure 10-fT signals of interest on top of 1-μT interference, one would need a sensor with a dynamic range exceeding 8 orders of magnitude. To date, no magnetic sensor exists with a linear response over such a wide dynamic range. The linearity of the sensors, on the other hand, is a necessary prerequisite for successful signal processing and source analysis. Therefore, an efficient means to reduce the

actual physical magnetic interference is necessary for feasible MEG recordings and analysis, especially in a clinical environment. When hardware-based magnetic shielding is sufficient to keep the sensors within their linear operating range, the remaining interference can be further reduced by multichannel signal processing methods, such as spatial and temporal filtering.

Another challenge specific to MEG is the possible movement of the subject's head during recording. The physical sensor array of the MEG system is stationary. Movement-related distortion of the signal biases source localization and is more challenging with MEG than with the EEG method where the electrodes are attached on the scalp and do not move with respect to brain. To fully benefit from the MEG method's better source localization capability, one must ensure that the accurate location of the head relative to the sensor array is known at all times during the MEG recording.

1.4 Sources of Interference and Noise

The largest-amplitude ambient magnetic fields usually arise from traffic outside of the building. Elevators and MRI magnets operated close to MEG, and even doors made of magnetic material are potential sources of magnetic interference inside of the building. In urban environments, cars on nearby streets, trains and metros cause low-frequency peak-to-peak variations of magnetic field which are typically in the range 1–3μT.

When a vehicle moves at a distance of D with velocity v, the frequency range of the resulting interference is around v/D. For example, cars driving at 50 km/h at a distance of 30 m or a train passing by at 200 km/h at a distance of 100 m result in low-frequency field variations at around 0.5 Hz.

In this frequency range the shielding factor of a typical magnetically shielded room (MSR) is rather low, about 100 (40 dB). Therefore, operating magnetometer sensors in an MSR with 1-μT ambient interference from traffic requires sensors with higher than 10-nT dynamic range, if no other means of interference rejection is used.

Because the shielding factor of an MSR rises steeply with increasing frequency, the low-frequency interference present in the environment will typically dictate the required hardware shielding performance at a specific MEG site. For example, interference at powerline frequencies 50/60 Hz seldom exceeds 1μT in clinical environments, and is thus sufficiently dampened by a typical MSR which easily attains a shielding factor in the range of 10^5 (100 dB) at these frequencies. An example of low- and line-frequency interference inside a magnetically shielded room is shown in Fig. 1.

At radio frequencies up to several GHz, an MSR should maintain a shielding factor of about 10^5 or higher. Although these frequencies are much higher than any brain signals and thus irrelevant for MEG, the shielding is still required because the functioning of DC SQUIDs involves intrinsic frequencies in the GHz range, related

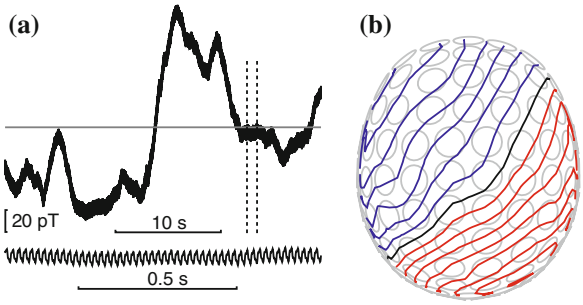

Fig. 1 **a** An example of a single magnetometer (over the occipital region) signal recorded without a subject in the magnetically shielded room. The inset shows a 1-s epoch of the data which reveals the line-frequency contamination. **b** Spatial distribution at the time of the largest amplitude of the signal shows a homogeneous field distribution. The view is from the top of the sensor array, and the *circles* indicate the locations of the 102 magnetometers of the Elekta Neuromag MEG system. *Blue* and *red lines* indicate magnetic field flux into and out of the array surface, respectively. The step between adjacent contour lines is 20 pT

to the superconducting tunnel junctions whose so-called Josephson frequency is at 4.8 GHz for a bias voltage of 10 μV (see, e.g., Clarke and Braginski 2006). Modern digital equipment may cause strong electromagnetic radiation in this frequency range, and would severely disturb unshielded SQUID-based sensors.

The sources of interference and noise mentioned above are related to the installation site of the MEG device. In addition, there are numerous interference sources that are related to the MEG technology itself. Some of them cannot be compensated for by the MSR because they stem from the MSR itself or from sources inside of the MSR. For example, the walls of the MSR are made of conductive and magnetic material, which may result in magnetic interference by two mechanisms. The thermal currents in the walls of a typical MSR generate a magnetic field noise density of about 2 fT/$\sqrt{\text{Hz}}$ (Nenonen et al. 1996). Also, small vibrations of the walls result in magnetic interference typically seen as 10–30-pT peaks in the frequency band 13–30 Hz. These peaks result from the high-Q-value eigenmodes of the MSR walls and ceiling that are driven by the vibration of the building and the infrasound due to forced ventilation.

Another vibration-related artifact in MEG signals arises from the mechanical movement of the MEG device itself in the remanence field inside of the MSR. The maximal amplitude of this type of artifact in magnetometer sensors can be estimated by multiplying the remanence field by the vibration-related rotation angle. The remanence field in a typical MSR is 100 nT. Assuming the vibrational rotation to be a 10-μm movement of the sensor helmet around an axis one meter away from the helmet, we observe 1 pT magnetic signal due to this vibration.

All metal, magnetic or conductive, components of the MEG device are potential sources of magnetic interference. Most of these sources can be eliminated by proper design of the equipment. After careful design, the dominant device-related source of magnetic interference is typically the thermal insulation (super

insulation) covering the sensor area of the dewar, which is necessary to keep the liquid helium boil-off rate below 10 l per day. In modern MEG devices this noise contribution is below 3 fT/$\sqrt{\text{Hz}}$. Any auxiliary devices such as stimulators, cameras, speakers or microphones used inside of the MSR are also potential sources of severe interference. The compatibility of these devices with the MEG method must be carefully verified case by case.

Finally, the recorded MEG signals contain sensor noise related to the SQUIDs and their readout electronics. The pick-up antennas in a modern MEG device, having about 300 sensors in total, are relatively small. Therefore, to achieve adequate field sensitivity, it is necessary to minimize the electronics-related noise contribution. This can be done, for example, by applying pre-amplifier noise cancellation based on positive feedback (Kiviranta and Seppä 1995). In this way, the noise in individual MEG channels can be kept at the level of 3–4 fT/$\sqrt{\text{Hz}}$ in the white noise range and at about (6/*f*) fT/$\sqrt{\text{Hz}}$ at low frequencies (1/*f*-noise). There are also other device-related non-idealities that manifest as distortion and bias in the recorded data. Such factors include, for example, errors in calibration, location, and orientation of individual sensors, as well as imbalance of gradiometers and cross-talk between the channels. Most of these non-idealities, often seen as a kind of "DC-interference", can be well characterized and compensated for by modern software methods that are discussed in detail in Sect. 3.

In addition to the ambient and device-related noise and interference mechanisms described above, the subject studied—or patient in case of clinical MEG—may also be a source of severe interference. This applies especially in clinical work where patients may often have dental braces, therapeutic stimulators, or magnetic residue from prior surgical operations on or inside the skull. Prior to the invention of advanced software-based methods for interference rejection, such magnetic components in the body were considered a contraindication for a meaningful MEG study. The software methods to suppress disturbances caused by magnetism in patients are discussed in detail in Sect. 3.

2 Conventional Interference Reduction Methods

2.1 Magnetic Shielding

As mentioned in the previous section, the basic method of interference reduction that has been in use since the very beginning of neuromagnetic studies (Cohen 1970) is to use a magnetically shielded room (MSR). Figure 2 illustrates the principle of magnetic shielding and shows a commercial three-layer room. MSR is a room-size metal enclosure constructed using layers of both highly conductive metal, usually aluminum or copper, and metal with high permeability (see e.g. Kelhä et al. 1982). Mu-metal is a commercial name for a variety of nickel-iron alloys having a dynamic (initial) relative permeability as high as 50,000.

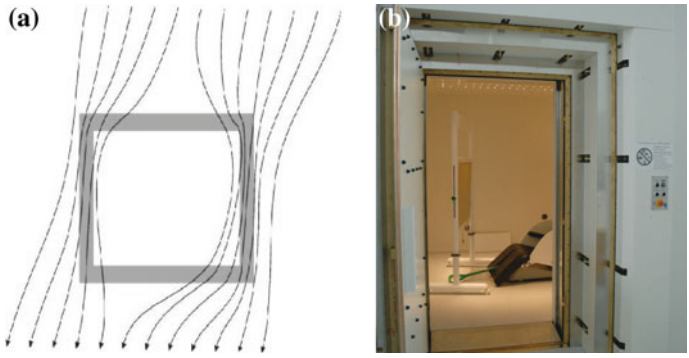

Fig. 2 **a** Principle of magnetic shielding. Layers of aluminum and mu-metal provide a path for magnetic field lines around the enclosure. **b** A three-layer magnetically shielded room (Imedco AG, Hägendorf, Switzerland) at the O.V. Lounasmaa Laboratory of Aalto University (Espoo, Finland)

The shielding performance of a MSR is usually described by a frequency-dependent shielding factor which is the ratio between the external interference field $B_{\text{ext}}(f)$ and the corresponding value of field inside of the shield $B_{\text{in}}(f)$, that is, $S(f) = B_{\text{ext}}(f)/B_{\text{in}}(f)$. The shielding effect of a metallic magnetic shield made of conducting and high-permeability material is based on two mechanisms: polarization of the high-permeability metal, and eddy currents induced by varying magnetic field. These mechanisms are demonstrated in Fig. 3 where the shielding performances of different wall compositions, with equal proportions of mu-metal and aluminum, are compared.

At frequencies below 0.1 Hz, where induction is negligible, the polarization of the high-permeability material is the only mechanism providing magnetic shielding. When the frequency increases, the induction mechanism starts to have an effect on the shielding. In this frequency range, additional shielding is provided by the "global" eddy currents induced to run in the conducting walls around the entire room. This additional shielding effect sets in at the frequency determined by the resistance of the conductive wall and the inductance related to these "global" currents. The related shielding effect grows proportional to the frequency, as shown by the lowermost $S(f)$-curve in Fig. 3. When the frequency is further increased, the induced currents on the outer surface of the wall start to shield the inner parts of the wall, and the shielding starts to grow exponentially with increasing frequency. This is the well-known skin effect, with a skin depth given by $\delta = 1/\sqrt{\pi f \mu \sigma}$. Here σ and μ are the conductivity and permeability of the wall.

Since the construction of the first room-size magnetic shield in 1962 (Patton and Fitch 1962), a variety of different multilayer MSRs have been manufactured for biomagnetic purposes. To obtain increasingly better magnetic shielding performance, the amount of metal and the number of metal layers has been increased up to the record number of eight (Bork et al. 2001). Such a huge MSR with $6 \times 6 \times 6$ m^3 external dimensions and a total of 24.3 tons of mu-metal provides

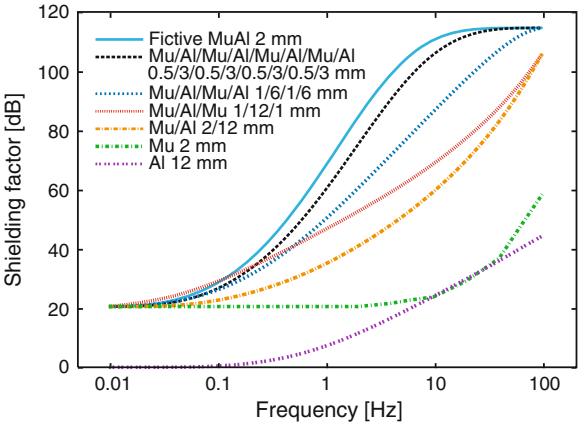

Fig. 3 Optimization of aluminum/mumetal-based MSR wall structure. Estimated shielding factors of four different Al/mu-sandwich structures are shown. The scattering matrix model for concentric spherical shells (e.g., Kelhä et al. 1982) with inside radius 1.9 m is used in the calculation. The layers in the 2-, 3-, 4-, and 8-layer sandwiches are in surface-to-surface contact, and the amount of metal is kept constant in all four structures; 2 mm of mu-metal and 12 mm of aluminum in total. For the electrical conductivity of aluminum and mu-metal, and for the relative permeability of mu-metal we have used $3.57 \times 10^7 (\Omega\mathrm{m})^{-1}$, $1.82 \times 10^6 (\Omega\mathrm{m})^{-1}$, and 16,000, respectively. For reference, the $S(f)$-curves of 12 mm of mere aluminum, and 2 mm of mere mu-metal are shown by the two lowermost *curves*. For mere aluminum, the shielding is negligible below 0.1 Hz, and above that grows proportional to f due to induced global eddy currents. The skin depth of aluminum is so long that no skin effect, that is, exponential growth of $S(f)$, is evident even at 100 Hz. This is because of the low relative permeability of aluminum. The second lowest curve is for 2-mm mu-metal showing a 20-dB shielding down to DC but no global current shielding regime, because of low electrical conductivity of mu-metal. Instead, a skin effect regime with exponential growth of $S(f)$ is starting to show up above 10 Hz. Keeping the total amount of metal constant, but increasing the number of layers in the al/mu-sandwich reduces the skin depth and the frequency at which the skin effect sets in. With an increasing number of layers in the sandwich, the shielding factor at a given frequency between 0.5 and 100 Hz increases and the $S(f)$-curves asymptotically approach the uppermost curve showing the shielding obtained with an "infinite number" of layers, that is, a 2-mm thick shell made of fictive "Al/mu-alloy" having the electrical conductivity of a 12-mm thick aluminum plate, and the relative permeability of mu-metal. The saturation of $S(f)$ at 115 dB is due to the openings in the MSR wall

excellent magnetic shielding even at very low frequencies. While this type of shielding is extremely useful in scientific research requiring magnetically disturbance free environments, it is not practical for clinical MEG use.

As a solution for the need of compact and lightweight MSRs for clinical MEG applications, designs with a total MSR weight below 5 tons and external dimensions of $3 \times 4 \times 2.5$ m^3 have been developed during the past ten years (for performance evaluations, see Parkkonen et al. (2006) and de Tiège et al. (2008)). To ensure sufficient shielding performance of these light MSRs with reduced amount of mu-metal, special attention has been paid to the joints between the metal wall elements to guarantee optimal electric and magnetic conductance

across the joints (Simola et al. 2005). Also, several conductive aluminum layers and high-permeability mu-metal layers have been interleaved to reduce the effective skin depth of the wall structure (Simola 2003). This lowers the frequency at which the skin effect and the related exponential growth of the shielding factor $S(f)$ with increasing frequency sets in, thus increasing the shielding performance at frequencies above 0.5 Hz; see Fig. 3.

To support the magnetic shielding provided by a MSR, several active shielding concepts have been proposed and realized. The simplest method to actively counteract ambient magnetic interference consists of a magnetic sensor—a three-axis fluxgate, for example—located in the vicinity of the MSR, and three orthogonal sets of coils wound on the outside of the MSR. The fluxgate records the variations of the ambient field and controls a current supply that feeds the coil sets to produce a field that counteracts the ambient field variations at the location of the MSR. This method is called feedforward active compensation. In this arrangement the fluxgate has to be located far from any local sources within the building, and at a sufficient distance from the compensation coils. The feedforward system works well against distant interference sources that produce a nearly uniform field. With this method a typical achievable shielding factor against such interference is in the range 10–50 (20–35 dB).

If the fluxgate is moved closer to or within the coil system, the arrangement turns into a feedback system that keeps the magnetic field constant at the location of the fluxgate, providing an alternative approach to construct an active compensation system. The fluxgate cannot be located inside the MSR because the inductive time constant of the MSR leads to a relatively long time delay between $B_{\text{ext}}(t)$ and $B_{\text{in}}(t)$, typically 2–3 s. A novel feedback active compensation method based on the MEG sensors and compensation coils inside the MSR will be described below in Sect. 3.5.5.

2.2 Gradiometrization

Another hardware-related interference rejection method, which has been utilized since the early days of biomagnetism, is the use of gradiometers instead of simple magnetometers. Zimmerman and Frederick (1971) used an axial gradiometer consisting of two oppositely wound co-axial coils, while Cohen (1979) utilized a planar gradiometer where the coils are on the same plane (see Fig. 4).

A first-order gradiometer has a pick-up antenna consisting of two loops that are planar, parallel, and usually identical in size and shape. The loops are oppositely wound and located in space so that one loop is translated from the other by a vector $\mathbf{h}$. The length h is called the baseline of the gradiometer. If $\mathbf{h}$ is parallel to the common normal $\mathbf{n}$ of the loops, the gradiometer is called axial. In the case of a planar gradiometer, $\mathbf{h}$ is orthogonal to $\mathbf{n}$. In principle, $\mathbf{h}$ and $\mathbf{n}$ could be at any angle relative to each other but axial and planar are the two gradiometer types most commonly used.

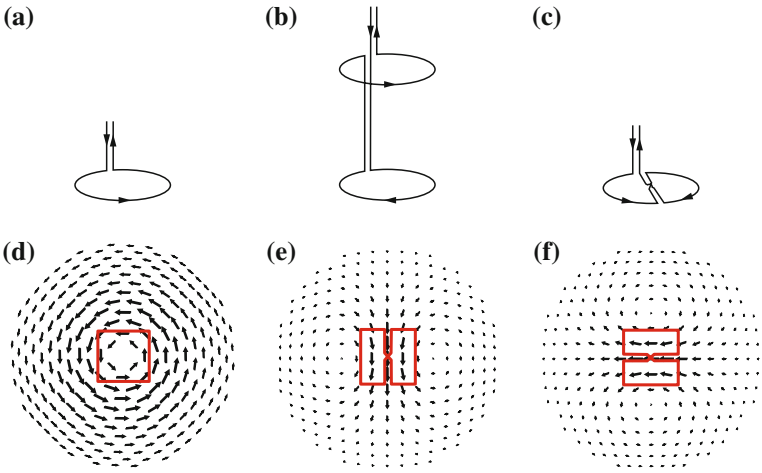

Fig. 4 Some pick-up coil geometries: **a** magnetometer, **b** co-axial first-order gradiometer, and **c** planar first-order gradiometer. The leadfield, or sensitivity, patterns of **d** magnetometer and axial gradiometer measuring B_z, **e** planar gradiometer measuring dB_z/dx, and **f** planar gradiometer measuring dB_z/dy

The signal of a gradiometer MEG channel is proportional to the net magnetic flux through the pick-up antenna. If the field contains gradients up to second order only and the gradiometer is ideal this flux is given by

$$g = A\mathbf{n}^T \begin{pmatrix} \partial B_x/\partial x & \partial B_x/\partial y & \partial B_x/\partial z \\ \partial B_y/\partial x & \partial B_y/\partial y & \partial B_y/\partial z \\ \partial B_z/\partial x & \partial B_z/\partial y & \partial B_z/\partial z \end{pmatrix} \mathbf{h} \tag{1}$$

where A is the area of one gradiometer loop.

For geometrical reasons, gradiometer antennas composed of identical oppositely-wound loops are totally insensitive to a uniform field of any direction. Consequently, they rather effectively reject interference from any sources far away from the MEG device. In practice, the interference rejection ratio of gradiometers is limited by the fact that a typical interference field is not exactly uniform, and that the geometry of the gradiometer is not ideal. The geometric non-ideality of a gradiometer is called imbalance. The signals from near-by sources, the brain signals, are highly non-uniform and therefore attenuated only slightly. Typically, for a gradiometer in a MSR, the signal-to-interference ratio for ambient interference is approximately by a factor of 100 higher than for simple magnetometers.

The interference signal in ideal gradiometers, related to relatively smooth interference fields, is well described by Eq. (1). When dealing with the signals of interest in MEG, which are related to neural current distributions, the signal in a MEG channel is better described by using the concept of a lead field $\mathbf{L}(\mathbf{r})$, defined by the expression

$$b_k = \int_{v'} \mathbf{L}_k(\mathbf{r}') \cdot \mathbf{J}(\mathbf{r}')dv' \tag{2}$$

where the output of channel k, b_k, is obtained as the projection of the current distribution $\mathbf{J}(\mathbf{r}')$ on the lead field, or sensitivity pattern, $\mathbf{L}_k(\mathbf{r}')$.

The two types of gradiometers, axial and planar, have different sensitivity patterns (Fig. 4). An axial gradiometer has a similar lead field as a magnetometer: zero for sources directly under the sensor, otherwise wide circular pattern with the maximum sensitivity some distance sideways. Thus, a single axial gradiometer can detect neuromagnetic signals from a wide region in the brain, but is also sensitive to interference caused by sources near to the sensor. Planar gradiometers in turn have very compact lead fields, which exhibit the maximum directly under the sensor.

2.3 From Single-Channel to Multichannel MEG

In the early days of biomagnetism, MEG devices were comprised of one sensor channel only. Any feature in the signal could be from the brain, environment, or electronics. Instrumentation developed during the years, and the number and size of the sensor arrays increased gradually. Figure 5 illustrates the evolution of multichannel MEG sensor array from a small-size four-channel axial gradiometer to 306-channel whole-head system combining magnetometers and planar gradiometers. Modern whole-head MEG arrays have facilitated development of effective multichannel signal processing and analysis methods, which are discussed in Sect. 3. Design of multichannel sensor arrays involves several parameters, such as the number of channels, geometry of the pick-up coils, internal noise level of the sensors and so on. Detailed comparisons of the advantages and disadvantages of the arrays of axial and planar sensor types have been presented in the literature (Ahonen et al. 1993; Vrba and Robinson 2002; Nenonen et al. 2004).

2.4 Reference Sensors

A method distantly related to the gradiometer concept is the use of reference sensors, which consists of an array of extra magnetic sensors located typically 20 cm above the MEG sensor helmet. The idea is that the reference sensors are so far from the source of interesting signals that they only detect interference. This measured interference can be modeled, either by a physical model or statistically, and then subtracted with proper weighting coefficients from the signals of the MEG channels. Because of the required extra hardware and the modeling and subtraction, the reference sensor method can be considered a combined hardware/software method.

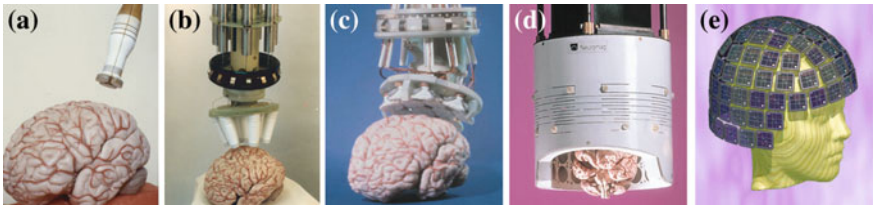

Fig. 5 Evolution of MEG devices: **a** 4-channel axial gradiometer system, **b** 7-channel axial gradiometer system, **c** 24-channel planar gradiometer array, **d** 122-channel planar gradiometer helmet, **e** 306-channel whole-head system combining 102 magnetometers and 204 planar gradiometers. (**a**–**d**: Courtesy of Dr Jukka Knuutila, Elekta Oy; **e**: Courtesy of Dr Mika Seppä, O.V. Lounasmaa Laboratory, Aalto University)

In the reference-sensor method the interference contribution at the primary MEG sensors is extrapolated from the signals in the reference sensors by expanding the magnetic field into a Taylor series about the origin at the primary sensor. Synthetic first-, second- and third-order gradiometers can be formed in this manner (Vrba and Robinson 2001). Magnetometers and gradiometers can serve both as primary and as reference sensors. Synthetic third-order gradiometers reduce the environmental interference substantially. In order to avoid increasing the sensor noise, the reference sensors should have a higher gain than the primary sensors. Synthetic gradiometers have been demonstrated to operate even without a magnetically shielded room in an environment with low magnetic interference level.

2.5 Limitations

All the traditional interference rejection methods described above are in use at many MEG sites and have proven to work and to be sufficient in most cases to enable proper functioning of the MEG device. The main problem with the passive shielding method is the large size, heavy weight and high price of the MSR. Also, the need to isolate the patient behind a closed door may hamper clinical work. Lighter passive magnetic shields would boost the clinical use of MEG.

A relatively simple way to assist passive shielding is to use feedforward active compensation. The basic problem with this method of active compensation is related to the local sources in the vicinity of the MSR and the fluxgate sensor. If there are many such sources, it is impossible to set the system up properly and the arrangement may even amplify the interference from sources close to the fluxgate.

The basic shortcoming of the reference sensor method is related to the fact that the interference inside of the MSR may still be 1,000 times higher than the brain signals. Therefore, to be able to properly subtract the interference, one should know it at the location of each sensor with an accuracy better than one per mille (0.001). This is not possible when the interference needs to be extrapolated from the signals of only 10–30 reference sensors located at a 20-cm distance from the primary MEG sensors.

The conclusion is that improved interference rejection methods are needed, specifically to develop MEG towards clinical use. For clinical installations, it is not always possible to select the magnetically most silent location in the hospital. Also, clinical patients cannot be chosen for subjects as freely as in basic neuroscientific research. Patients may also have therapeutic stimulators that are magnetic or there may be magnetic residue from previous surgery in their body. In addition, patients and healthy volunteers often show interference from biological sources such as the eyes and cardiac muscle; see Parkkonen and Salmelin (2010) for typical examples. None of the methods described above are useful against such interference.

3 Modern Approaches to Noise Reduction

3.1 Mathematical Representation of Multichannel MEG Signals

We will concentrate on mathematical noise reduction methods and start from the basic principles of computational signal representation. These basic concepts are a necessary prerequisite for the understanding of novel algorithms used in MEG today.

As explained above, a common way to express the signals of individual MEG channels is the leadfield representation of Eq. (2), which shows how the output of channel k, b_k, is obtained from the current distribution $\mathbf{J}(\mathbf{r}')$ as the projection of the current distribution to the lead field, or sensitivity pattern, $\mathbf{L}_k(\mathbf{r}')$. MEG sensors are sensitive to both neural currents and currents related to interference but usually the lead fields are computed for neural currents only with the assumption that the measured data are sufficiently clean. Figure 4 shows examples of lead fields of magnetometer and gradiometer channels. The wide-spread sensitivity pattern of the magnetometer indicates that the magnetometer picks up signal from a large portion of the source volume, including deep structures in the brain. Similarly, magnetometers are also quite sensitive to external interference signals, which are spatially relatively uniform. On the other hand, the gradiometer channels are very focal and most sensitive to the superficial parts of the brain and insensitive to homogeneous interference fields.

Modern MEG devices contain hundreds of channels and the whole sensor array discretizes the continuous field distribution into a signal vector $s(t) = [s_1(t)\, s_2(t) \ldots s_N(t)]$ at any given time t. This N-dimensional vector representation allows us to utilize linear algebra in the signal processing of MEG. From now on, we will call the set of measurable signal vectors the *signal space* of MEG and show that different subspaces can be distinguished in the signal space. The concept of signal space was first introduced in MEG already in the 1980s (Ilmoniemi 1981; Ilmoniemi and Williamson 1987; Ilmoniemi et al. 1987) and it has thereafter been the basis of several efficient signal processing algorithms.

3.2 Common Distortion Mechanisms of MEG Signals

The basis of any model applied to a multichannel MEG recording is the assumption that the sensors can be considered independent. For example, according to this assumption, a particular forward model can be computed by evaluating the magnetic flux at individual sensors merely based on the geometry of the associated source model and the sensor itself without considering the signals of other sensors. In reality, however, sensors always have some degree of coupling between each other. Therefore, instead of measuring the pure magnetic flux ϕ_i, channel i detects the distorted signal $\phi_i^{'}$ due to the coupling of all other channels through the so-called cross-talk coefficients k_{ij}, i.e.,

$$\phi_i^{'} = \phi_i + \sum_{j=1}^{N} k_{ij}\phi_j^{'}, \tag{3}$$

where $k_{ii} = 0$. Cross-talk arises e.g. from mutual inductance between sensors or electronics-based couplings. An efficient way to reduce cross-talk is to keep the current of the pick-up coils at zero by feedback, which eliminates the inductive coupling between the pick-up coils. Some cross-talk, however, always exists and it is important to estimate the coefficients k_{ij} either computationally or to measure them directly by sequentially feeding a current to each sensor and detecting the response of other channels to this test current (Taulu 2000). Computational means include a model for the mutual inductance between sensors, which can be based, e.g., on analytical formulae between wire elements of the flux transformers. Once the coefficients k_{ij} have been determined, the above equation can be written in the matrix form

$$\phi^{'} = \phi + K\phi^{'} \tag{4}$$

from which the cross-talk-corrected estimate can be computed as

$$\phi = (I - K)\phi^{'}. \tag{5}$$

In addition to the cross-talk, hardware-originating signal distortion arises due to errors in the calibration coefficients and geometrical imprecision, such as position and orientation errors of the sensors, and imbalance of gradiometers. If the expected field-to-voltage calibration coefficient of channel i is c_i and it deviates from the true calibration c_{0i} as $c_{0i} = c_{\varepsilon i}c_i$, then the corrected signals can be computed as

$$\phi_c = C\phi = C(I - K)\phi^{'}, \tag{6}$$

where C is a diagonal matrix containing the estimated relative calibration coefficients:

$$C = diag(c_{\varepsilon 1} \;\; c_{\varepsilon 2} \;\; \ldots \;\; c_{\varepsilon N}). \tag{7}$$

Thus, the hardware-based distortions such as cross-talk and scalar calibration errors can be compensated for by simple linear operations. The geometric corrections mentioned above have to be incorporated into more complex models that are applied to the acquired and compensated data ϕ_c. Several calibration algorithms have been introduced in MEG (Hall Barbosa et al. 1999; Ornelas et al. 2003; Chella et al. 2012). State-of-the-art calibration accuracy ensures a good match between the measured data and the models, such as the forward fields corresponding to neural currents or models used in interference suppression algorithms.

The distortion mechanisms described above are always present in MEG recordings, even in an ideal environment with no actual interference or noise. In addition, MEG signals always contain random sensor noise or radiation-shield noise, and almost always contain external interference. Quite often disturbances related to the subject or patient are embedded within the signal as well. In the following, we divide the interference and noise of MEG into three groups:

1. Interference from far-away sources; spatially smooth field patterns corresponding to sources relatively far from the sensor array. In an empty MSR, these sources contain currents on the walls of the MSR induced by external interference fields.
2. Interference from near-by sources; spatially complex field patterns due to the proximity of the sources.
3. Random noise intrinsic to the MEG device itself, i.e., sensor noise and sensor artifacts.

In addition to the spatial categories above, different interference types may also have specific time–frequency characteristics that can be utilized in the interference suppression approaches. MSR only attenuates interference of category 1 and therefore MEG measurements have traditionally been conducted only with cooperative subjects who are able to stay still and who have no magnetic material in their body. In clinical settings, however, it is not practical to request or rely on complete immobility of the patient. Even the slightest movements due to respiration or heart beat can cause severe movement artifacts in the presence of magnetized material related to, e.g., dental braces, tiny magnetic residues in the body, or therapeutic stimulators. Thus, signal processing methods are needed to compensate for category 2 interference. Intrinsic sensor noise (category 3) is always present in any MEG recording and its contribution is typically taken into account in the source modelling phase in the form of a covariance matrix but recently new pre-processing methods to reduce sensor noise have also been proposed.

3.3 Physics- and Statistics-Based Detection of Interference

Many interference suppression methods are based on physical or statistical models of the measured signals. The former methods typically utilize a model that aims to explain the signals in physical terms such as sources while the latter methods often consist of finding some statistical features from actual data recorded with the MEG system. In the following, we will use two signal space methods as examples of the statistical and physical approaches and explain their benefits and drawbacks.

The Signal Space Projection (SSP) (Uusitalo and Ilmoniemi 1997) and Signal Space Separation (SSS) (Taulu et al. 2004) methods utilize the ample spatial oversampling of the neuromagnetic field in a modern MEG device with hundreds of channels. At a typical brain-to-sensor distance in MEG ($\sim$3 cm), the magnetic field from neural sources has less than 100 degrees of freedom (independent geometric shapes) that can be resolved above the sensor noise.

The SSP method is based on statistical analysis of the recorded interference signal. The interference is recorded with no subject in the MEG device. A principal component analysis is made on this "empty-room recording" containing only interference and sensor noise.

In the SSP method, the signal recorded by an N-channel device from the subject is projected on the $(N - n)$-dimensional subspace that is orthogonal to the first n principal components—those with the largest eigenvalues—of the empty-room recording. Assuming that the ambient interference is a result from a reasonably stable statistical process this projection leaves us with relatively interference free $(N - n)$-dimensional MEG data. The brain signal is also slightly distorted by the projection operation but this can be taken into account in a simple manner in the subsequent signal analysis (Uusitalo and Ilmoniemi 1997).

SSP is a purely statistical method and therefore does not suffer from any calibration inaccuracy in the sensor array, as long as the calibration of the sensors and the geometry of the sensor array stays constant. Being an orthogonal projection method SSP does not increase the individual sensor noise (rather it decreases the noise slightly) but causes some distortion of the spatial pattern of the signal. Specifically, signals from very deep sources are reduced in amplitude as they have a significant projection on to typical ambient interference directions in the signal space.

Contrary to the SSP method, which is statistical, the SSS method is based on the physics of magnetic fields, i.e., Maxwell's equations (Taulu et al. 2004). In this method, the signal space is provided with a basis that encompasses all physically possible magnetic field distributions (solutions of Maxwell's equations in a space free of magnetic material). The measured signals can be uniquely represented in this basis. By simple physical arguments the field shapes can be classified into two groups: field shapes corresponding to sources inside of the sensor array, and those corresponding to sources outside of the array. In this way, two linear subspaces of the signal space can be defined: S_{in} for inside sources and S_{out} for outside sources. The external interference can now be removed from the signals by simply estimating the contributions of S_{in} and S_{out} and subsequently leaving out the signal components in S_{out}.

The advantage of SSS over SSP is its generic nature as it is based on the physics of the magnetic field rather that statistics of the recorded interference. Because of this, SSS is universal and can handle also such new interference sources that we have no prior statistics on. SSS is not an orthogonal projection, and therefore it does not change the spatial patterns of the neuromagnetic signal. On the other hand, because SSS is based on a computational model, it is rather sensitive to the calibration accuracy of the MEG system (Nurminen et al. 2008).

3.4 Noise Reduction in the Spatial, Temporal, and Spectral Domains

3.4.1 Decomposition of MEG Signals

The data acquired with N_c channels over a period of time consisting of N_t samples can be represented as an $N_c \times N_t$-dimensional matrix Φ. Modern mathematical noise reduction methods are based on a *decomposition* of the high-dimensional data into some basis components that can be used in processing the data to suppress the contribution of unwanted interference signals. We can classify the basic decomposition approaches as follows:

1. Spatial decomposition: $\underset{N_c \times N_t}{\Phi} \rightarrow \underset{n \times N_t}{X}$
2. Spectral decomposition: $\underset{N_c \times N_t}{\Phi} \rightarrow \underset{N_c \times N_F}{F}$
3. Temporal decomposition: $\underset{N_c \times N_t}{\Phi} \rightarrow \underset{N_c \times N_F}{F} \underset{N_F \times N_t}{Y}$
4. Combination of the above: for example, $\underset{N_c \times N_t}{\Phi} \rightarrow \underset{n \times N_t}{X} \rightarrow \underset{n \times N_F}{F} \rightarrow \underset{n \times N_F}{F} \underset{N_F \times N_t}{Y}$

In the following, we will describe the general mathematical models and the consequences of these operations. We will also give some examples of methods belonging to the different categories. A more detailed description of these methods will be given in Sect. 3.5.

3.4.2 Benefits and Drawbacks of the Decomposition Methods

1. In the spatial decomposition, some spatial model is applied to the data in order to extract features of interest and to suppress the contribution of interference signals. This leads to a representation $\underset{n \times N_t}{X}$, which contains the time series of the n spatially relevant features with typically $n \leq N_c$. The decomposition may be performed through a matrix operation

$$X = A\Phi, \tag{8}$$

where A is an $n \times N_c$-dimensional spatial filter matrix that may be, e.g., in the form of an orthogonal or an oblique projection matrix. In the former case, one rotates the data in the signal space into a subspace free of interfering signals (Uusitalo and Ilmoniemi 1997; Parkkonen et al. 1999a). The latter case may be used to extract the interesting from interfering signals in a mathematically unique fashion, e.g., by the SSS method. The benefit of the spatial decomposition is that it preserves the temporal information of the signals and may generally allow a robust classification of signals into interesting and interfering contributions. The drawback is that spatial operations, if not specified properly, may lead to spatial bias of the interesting signal, and measurement errors not modeled by A may spread into the decomposed result X. An example of a measurement error is a malfunctioning sensor. Methods belonging to this category include, e.g., SSP and SSS, some ICA applications, and beamformer. The last method, however, involves a specific neural source model when constructing the spatial filter matrix A.

2. In the spectral decomposition, the data are transformed into the Fourier or some other relevant temporal components by the matrix operation

$$F = \Phi B, \tag{9}$$

where B is an $N_t \times N_F$-dimensional matrix that performs the Fourier transform for each channel separately. The benefit of the spectral decomposition is that the spatial pattern is preserved and no localization bias is thus introduced. The drawback is that the signals of interest and the interference are often in the same frequency range, mixed in such a way that their reliable separation is not possible. A traditional way to use the spectral decomposition is visual investigation of the spectra of individual sensors, the rows of matrix F, and subsequent notch filtering. An example of a mathematically more advanced method is the S3P (Ramirez et al. 2011) algorithm that builds a spatial orthogonal projection matrix based on the spectral decomposition of sensor-level data.

3. In the temporal decomposition, the sensor-level signals are re-calculated from the spectral components. This is done by reconstructing the time courses from the decomposed spectral components and the corresponding temporal basis functions as

$$\Phi = F' Y, \tag{10}$$

where F' is derived from F, e.g., by leaving out spectral components expected to correspond to interference, and Y contains the corresponding temporal patterns of these selected frequency components. The benefits and drawbacks of this approach are the same as in the case of spectral decomposition. An example of

spectrum-based temporal decomposition is simple temporal filtering (low-pass, high-pass, or band-pass). However, the decomposition does not have to be based on Fourier components but it could also be derived through a direct temporal extraction such as independent component analysis (ICA).

4. The above basic formalisms can be modified and combined in several ways. An example is the spatiotemporal signal space separation method (tSSS) that utilizes both the spatial filtering properties and temporal analysis to extract and suppress interference-related temporal forms. Combinations of ICA with short-time Fourier transforms have also been proposed to decompose MEG data into neurophysiologically relevant components (Hyvärinen et al. 2010; Ramkumar et al. 2012).

3.5 Review of Selected Novel Methods

In the following, we introduce a subset of various methods that can be used for interference suppression in multichannel MEG. This list of methods is not comprehensive but it rather shows examples on what the methods are typically based on. For guidelines on recommended practical use of interference and noise suppression methods, see, e.g., the guidelines publication by Gross and colleagues (2013) and the book chapter by Parkkonen and Salmelin (2010). Below, as examples of physical and statistical methods we describe the SSS and SSP methods in more detail.

3.5.1 Multichannel MEG

The signal space in single-channel MEG devices was trivial, one-dimensional, and spatial filtering was impossible. Any feature in the signal could be from the brain, environment, or electronics. The first step taken toward spatial filtering was the adoption of gradiometric sensors described in Sect. 2.2. Instead of measuring one field component at one point in space the field is measured also at an adjacent location. By subtracting the two measurements one reduces the interference signal from distant sources by a large factor, typically 100, but the reduction in the biomagnetic signal is relatively small if a proper base length is chosen for the gradiometer. The use of a gradiometer is an elementary signal space method. The two recordings made by the two pick-up loops of the gradiometer are two measurements, subtracted from each other to reject the common mode, which is dominantly due to ambient interference. This operation could be done by software but doing it by hardware, that is, by wiring a single gradiometer pick-up coil, gives the sensor a lot of extra dynamic range against uniform interference fields. The price paid is that the dimensionality of the signal space is reduced from two (the two loops) to one.

The possibility for actual spatial filtering opened up with the first multichannel devices. Already a two-gradiometer system helps one to further resolve biomagnetic signals and possible device-based artifacts. With an increasing number of channels the estimation and rejection of both ambient and device-based interference became easier.

However, the geometric complexity of the magnetic interference field over a volume as large as a typical MEG sensor array is potentially so high that actual spatial filtering used to recognize and remove ambient interference from the signals can be efficiently realized only when the number of channels is relatively high. This is because the magnetic field is a vector field in three dimensional space with three independent uniform components, five independent first derivatives, seven second derivatives etc. To determine interference fields up to second derivatives thus requires independent measurements done with 15 sensors. So, spatial filtering by gradiometrization up to second order derivatives would cut the signal space dimensions available for the actual brain signals in a 24 channel MEG device, say, down to $24 - 15 = 9$.

This is why efficient spatial filtering in MEG data processing has become available only when the number of channels has grown upward to several hundreds. On the other hand, when such a high number of channels is available, signal space methods based on linear algebra are a better way for interference rejection than, for example, reference sensor systems, for the following reason. The interference field is usually much higher in amplitude than the neuromagnetic signal. Therefore, it must be determined with the best possible accuracy. The optimal way to do this is to use the entire set of sensors instead of the relatively few reference sensors, to record the interference. A further advantage in this approach is that the interference is now recorded at the very locations where we want to know it. No spatial extrapolation is needed, which improves accuracy of the interference estimate. In the signal space approach both interference and the biomagnetic signal are mixed up in the signals from the same set of channels but they can still be separated with appropriate signal space methods.

3.5.2 The SSP Method

The signal space projection method is set up for suppressing ambient magnetic interference by recording MEG data without a subject for a few minutes. In this situation it is certain that all recorded signal is interference. This multichannel signal is then statistically analyzed by using principal component analysis (PCA). The dominant n PCA-components give the signal space directions containing the largest-variance magnetic interference field patterns. These orthonormal signal vectors are then organized as an $N \times n$-dimensional matrix E_n and the orthogonal projection operator is formed as:

$$P_{\text{orth}} = I - E_n E_n^T, \tag{11}$$

where I is an $N \times N$-dimensional identity matrix. Then, the recorded N-channel MEG signal is projected on the $(N–n)$-dimensional signal subspace that is orthogonal to all the directions corresponding to the n dominant PCA components:

$$\phi_{\text{orth}} = P_{\text{orth}} \phi \tag{12}$$

Experience on using the SSP method at several MEG sites over 15 years has shown that the ambient interference field patterns are relatively stable over several years. SSP projection operator (with $n = 8$) determined from one 2-min recording is typically able to reduce interference amplitude in magnetometer sensors by a factor of about 300–1,000 (50–60 dB) when applied to the 2-min recording itself. In MEG recordings made at the same site even several years later, the same projection operation still suppresses interference by a factor of 100 at least.

This surprising stability of the interference patterns is partly due to the MSR. The strongest interference usually comes from distant sources which expose the MSR to relatively uniform magnetic fields. The MSR transforms these uniform fields into field patterns inside the MSR, which are not necessarily uniform but rather represent a kind of fingerprint characteristic for each room. Any new far-away source will cause a new, nearly uniform ambient field, which very closely resembles some linear combination of the interference fields due to earlier far-away sources, and thus produces a field pattern inside the MSR that approximately falls into the same interference subspace that is spanned by the dominant PCA-components in the earlier empty-room recording. We tested this MSR effect by introducing a novel interference source (an oscillating magnetic dipole 8 m from the center of the MSR) and applied the previously-determined SSP operator to suppress it; the shielding factor against this novel source was still more than 100 (40 dB) for the tested frequencies of 0.5–30 Hz (Parkkonen et al. 1999b).

SSP can be characterized as a software-based "gradiometrization" method that transforms the sensor array into a generalized gradiometer which is insensitive to those field shapes that are recognized as dominant PCA-components in a recording of ambient interference. A recently developed variant of the SSP method is the S3P algorithm (Ramirez et al. 2011) that builds the orthogonal projection operator through a spectral decomposition. This is beneficial especially for suppressing artifacts with distinct frequency characteristics; the algorithm has been shown to be useful, e.g., in the suppression of the high-frequency artifact of the deep brain stimulator (DBS).

3.5.3 The Signal Space Separation Method (SSS)

Another example of spatial filtering is the signal space separation method (SSS) that utilizes quasistatic Maxwell's equations combined with the sampling theory and geometry of the MEG array (Taulu 2008). The idea is to create a basis that

allows a device-independent representation of the data, which is capable of significantly suppressing the distortions typical to MEG, and also compensating for head movements.

At any sensor location $\mathbf{r}$ on the sensor array, the magnetic field caused by any distribution of sources is given by a series expansion

$$\mathbf{B}(\mathbf{r}) = -\mu_0 \sum_{l=1}^{\infty} \sum_{m=-l}^{l} \alpha_{lm} \frac{\boldsymbol{v}_{lm}(\boldsymbol{\theta}, \boldsymbol{\varphi})}{r^{l+2}} - \mu_0 \sum_{l=1}^{\infty} \sum_{m=-l}^{l} \beta_{lm} r^{l-1} \boldsymbol{\omega}_{lm}(\theta, \varphi), \tag{13}$$

where $\boldsymbol{v}_{lm}(\theta, \varphi) = \sqrt{(l+1)(2l+1)}\mathbf{V}_{lm}(\theta, \varphi)$ and $\boldsymbol{\omega}_{lm}(\theta, \varphi) = \sqrt{l(2l+1)}\mathbf{W}_{lm}(\theta, \varphi)$ with $\mathbf{V}$ and $\mathbf{W}$ being the vector spherical harmonic functions (VSH) defined by Hill (Hill 1954; Arfken 1985). Here the monopole term $(l = 0)$ is left out due to relation $\nabla \cdot \mathbf{B} = 0$ being valid everywhere according to the present theory of electromagnetic fields (see, e.g., Jackson 1999). In principle, an MEG device, with its data analyzed by a model including $l = 0$, could be used as a magnetic monopole detector by including $l = 0$ and estimating its contribution in the measured signal.

The infinite series of Eq. (13) is the general solution for the magnetic field in free space, expressed in the spherical coordinate system. Similar expansions based on other coordinate systems can also be used, but because of the nearly spherical shape of the sensor array it is advantageous to use this expansion for the physically possible field shapes. Using the two indices, l and m, labeling the spherical harmonics, the field shapes can be ordered according to increasing spatial complexity.

The coefficients α_{lm} and β_{lm} are called multipole moments. This expansion compactly represents the contribution of all sources generating a magnetic field. The two different parts of the expansion having different r-dependencies cover the convergence and divergence requirements of the fields produced by sources in different volumes of the physical space. Let us set the origin of the expansion somewhere in the middle of the brain volume and let $r_{\min}$ and $r_{\max}$ be the distances of the closest and most distant sensor, respectively, from this origin (see Fig. 6). The field from a source in the volume containing the origin ($r' < r_{\min}$) must be non-singular when $r' > r_{\min}$. Similarly, the field generated by a source in the outside volume ($r' > r_{\max}$) must converge when $r' < r_{\max}$. Consequently, the first sum in Eq. (13) is sufficient to describe fields generated by sources with $r' < r_{\min}$, and similarly, the second sum is all that is needed for fields from sources with $r' > r_{\max}$. As can be seen from Fig. 6, by selecting the expansion origin in a suitable way, typically at the center of the volume enclosed by the sensor array, the contributions of the brain and interference sources are separated into the first and second sum of the expansion, respectively. Here we assume that there are no sources in the volume defined by $r_{\min} < r' < r_{\max}$.

The truncation of the expansion has been investigated theoretically in (Taulu and Kajola 2005) and experimentally in (Taulu et al. 2005; Nenonen et al. 2007). The truncation of the two expansions in Eq. (13) with $l = L_{\text{in}} = 8$ and $l = L_{\text{out}} = 3$

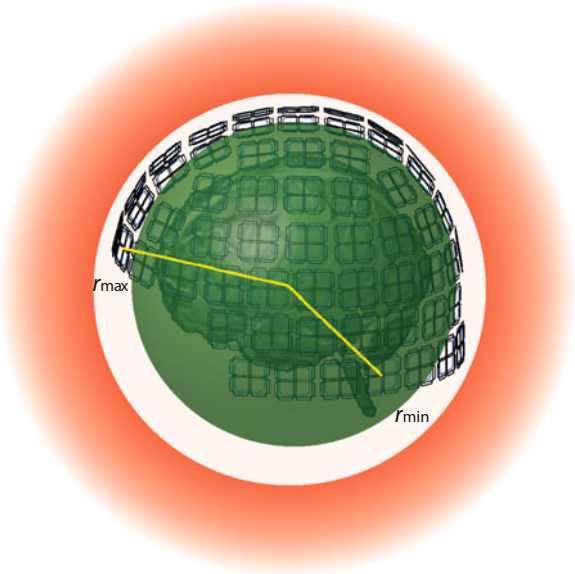

Fig. 6 Geometry of the signal space separation method

was found to be sufficient to ensure a negligible residual. Even in the case of 100 simultaneous current dipoles, $L_{\text{in}} = 8$ is enough to reconstruct the brain signal with an insignificant residual compared to sensor noise.

The basis vectors corresponding to each of the VSH functions are calculated by Eq. (13) giving us signal vectors a_{lm} and b_{lm} corresponding to the basis functions $-\mu_0 r^{-(l+2)} \boldsymbol{v}_{lm}$ and $-\mu_0 r^{l-1} \boldsymbol{\omega}_{lm}$, respectively. Thus, our linear model for any momentary signal vector ϕ, based on these basis vectors, is

$$\phi = Sx, \tag{14}$$

where the SSS basis $S = [S_{\text{in}} \;\; S_{\text{out}}]$ separates the internal and external contributions as

$$S_{\text{in}} = \left[a_{-1,1} \;\; a_{1,0} \;\; a_{1,1} \;\; \ldots \;\; a_{L_{\text{in}},L_{\text{in}}}\right] \tag{15}$$

and

$$S_{\text{out}} = \left[b_{-1,1} \;\; b_{1,0} \;\; b_{1,1} \;\; \ldots \;\; b_{L_{\text{out}},L_{\text{out}}}\right]. \tag{16}$$

The total number of spherical harmonics used in S_{in} and S_{out} must be smaller than the total number of channels. Otherwise the linear problem related to the coordinate representation in signal space becomes singular. The greater the margin (spatial oversampling) the more stable the solution of this linear problem becomes.

Since it is known that the number of measurable degrees of freedom in the neuromagnetic field—those exceeding the sensor noise—is below 100, it is usually

sufficient to map this field using spherical harmonics up to order $L_{\text{in}} = 8$. In most cases the field from external sources is sufficiently described by harmonic functions up to order $L_{\text{out}} = 3$. This corresponds to "gradiometrizing" the sensor array up to second-order derivatives of the interference field.

These relatively low expansion orders are sufficient because of the quite large distance between the sensors and sources of magnetic field in MEG. This applies to both the interesting and interfering sources. Because the series representing neural sources converges fast as a function of distance, fields with the highest spatial frequencies, corresponding to high l, are attenuated below sensor noise at the distance of the sensors when the sensor noise level of the present SQUID technology, about 3 fT/$\sqrt{\text{Hz}}$, is assumed.

In practice, modern multichannel MEG devices have a non-singular SSS basis since the sensors are located on a non-spherical surface and they are not strictly radial or tangential (Taulu 2008). Thus, we get a unique estimate for the device-independent coordinates in the form

$$\widehat{x} = S^{\dagger}\phi = \begin{bmatrix} \widehat{x}_{\text{in}} \\ \widehat{x}_{\text{out}} \end{bmatrix}, \tag{17}$$

where $S^{\dagger}$ is the pseudoinverse of S and the interference-suppressed estimate for the MEG signal can be calculated as

$$\widehat{\phi}_{\text{in}} = Re(S_{\text{in}}\widehat{x}_{\text{in}}). \tag{18}$$

By comparing Eqs. (8) and (17), we can see that SSS is a spatial filter with the model matrix $A = S^{\dagger}$.

Although the subspaces S_{in} and S_{out} are not orthogonal to each other, the contributions of the internal and external signals are not mixed in our estimated separation result, provided that our assumptions regarding sufficient values for L_{in} and L_{out} are correct and the system is calibrated accurately enough. The explanation for this is simple. Based on the theory of harmonic functions, the signal of a source in the volume $r' < r_{\text{min}}$ can be fully represented with the above expansion having non-zero α_{lm} coefficients and $\beta_{lm} = 0$. Similarly, for sources in the volume $r' > r_{\text{min}}$, the signal can be expressed with $\alpha_{lm} = 0$ and all β_{lm} being non-zero. On the other hand, the SSS basis S is linearly independent, which indicates that this obvious solution is also the only possible solution in the signal space.

Given a perfect calibration accuracy of the sensors and adequate spatial sampling, there is no mixing between the internal and external contributions because of the linear independence of the SSS basis vectors. Even with realistic calibration accuracy, this mixing is negligible if the expansion orders are sufficient.

All real measurements contain sensor noise. In MEG measurements, it is usually assumed that this noise is normally distributed and uncorrelated among the sensors, resulting in a diagonal covariance matrix. Application of SSS changes the sensor noise covariance $\mathbf{C}$ which can be taken into account if needed as shown in

(Taulu and Kajola 2005). The brain noise, which dominates over the sensor noise especially below 60 Hz, is not affected by SSS since it is produced by currents in the internal volume shown in Fig. 6.

The condition number, defined as the ratio of the largest and smallest singular value of the SSS basis, is apparently very high due to the highly different scales of the different basis functions leading to a large range of norms of the SSS basis vectors. The basis can be stabilized simply by normalizing S, which usually gives a reasonable condition number, as discussed in (Taulu et al. 2005). Further stabilization can be achieved by selecting only the basis functions that have strong enough coupling to the sensor array to exceed sensor noise (Nenonen et al. 2007). When using a normalized S, the estimated coordinates $\hat{x}_{in,lm}$ can be transformed to SI units by dividing them with the norms $||a_{lm}||$ of the non-normalized basis.

It should be noted that the numerical stability of the coordinate transformation from the recorded multichannel signal to the SSS basis depends on the degree of spatial oversampling. The noise in the SSS coordinates increases when the margin between the number of channels and the number of SSS coordinates becomes narrower. In case the values $L_{\text{in}} = 8$ and $L_{\text{out}} = 3$ are chosen, the total number of basis vectors in the SSS basis would be $(L_{\text{in}} + 1)^2 + (L_{\text{out}} + 1)^2 - 2 = 95 \ll 300$. This amount of spatial oversampling has turned out to be sufficient to prevent any significant rise in sensor noise.

As a method based on physics, SSS is sensitive to all kinds of calibration errors and cross talk between the MEG channels. For inteference sources more than 1.5 m away, the shielding performance of SSS is limited by the calibration accuracy. This effect can be utilized in the calibration of a MEG device: the orientation, sensitivity, and imbalance of gradiometers is fine-tuned by simply requiring that there is no signal left in S_{in} when SSS is applied to an empty-room recording. After fine-calibration by this method the asymptotic shielding factor against distant interference sources can be brought up to 200–300 (Taulu et al. 2005). In addition to external interference suppression and calibration adjustments, the SSS method has several important applications, such as standardization of the head position and different sensor configurations (Taulu 2008), head movement correction (Nenonen et al. 2012), and enhanced magnetic source imaging (Vrba et al. 2010). An example of the interference suppression by the SSP and SSS methods is presented in Fig. 7.

3.5.4 The Spatiotemporal Signal Space Separation Method (tSSS)

The spatial SSS performs in a satisfactory manner in typical MEG measurements. A good estimate $\hat{x}$ is guaranteed when deviations ϕ_ε of the signal from the model in Eq. (14) are insignificant. Taking the deviations into account, the model is of the form

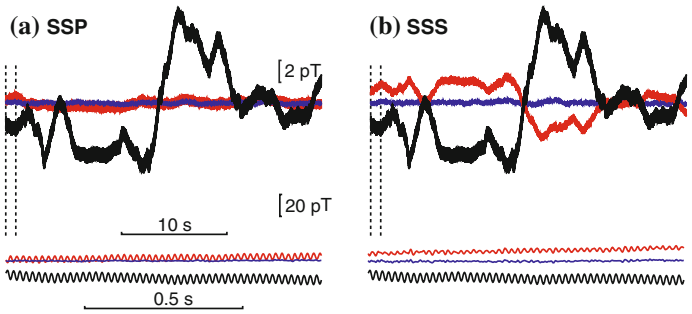

Fig. 7 Comparison of SSP and SSS with experimental data from an array with 102 magnetometers and 204 planar gradiometers. *Black curves*: raw data of a single magnetometer sensor above the occipital region recorded in an empty magnetically shielded room. **a** SSP: 5 generic SSP vectors (in *red*) and 8 SSP vectors computed from the same recording (in *blue*). **b** SSS: after SSS but without fine-calibration adjustment (in *red*) and after SSS and fine-calibration adjustment (in *blue*). The software shielding factor at the peak of the largest disturbance is 500. The *bottom* insets show a one-second epoch of the curves

$$\phi = Sx + \phi_\varepsilon \tag{19}$$

In addition to random sensor noise, such deviations can be produced by insufficient calibration accuracy of the sensor array causing erroneous elements in the basis matrix S. An additional source of deviation is the presence of sources that produce detectable magnetic fields with spatial frequencies higher than those included in the basis S, rendering the dimension of the basis matrix too small to correctly describe these fields. Such sources are typically artifactual sources in the immediate vicinity of the sensors, e.g., magnetized EEG electrodes close to the head.

From Eq. (19) we get the estimate

$$\hat{x} = S\phi = S^\dagger Sx + S^\dagger \phi_\varepsilon \equiv x + x_\varepsilon, \quad \text{where } x_\varepsilon = \begin{bmatrix} x_{\text{in},\varepsilon} \\ x_{\text{out},\varepsilon} \end{bmatrix} \tag{20}$$

Thus, the model misfit ϕ_ε leaks into the internal and external signal contribution estimated by SSS. This leakage can, however, be utilized in removing its contribution. Temporally, $x_{\text{in},\varepsilon}$ and $x_{\text{out},\varepsilon}$ contain equivalent temporal waveforms that were originally present in the signal deviation ϕ_ε. Assuming that the brain signals and external interference signals, both correctly modelled by the spatial SSS, are temporally uncorrelated, the only possible cause for temporal correlation between x_{in} and x_{out} is the above leakage phenomenon.

Removal of the contribution of ϕ_ε was developed and applied by Taulu and Simola (2006). First, the intersecting temporal waveforms are identified by a singular value decomposition (SVD)-based subspace intersection estimation method. Then, the intersecting waveforms are projected out in the time domain from the SSS estimate of the internal signal. Consequently, the recognized signal deviations, usually caused by nearby artifacts, are suppressed below the noise level

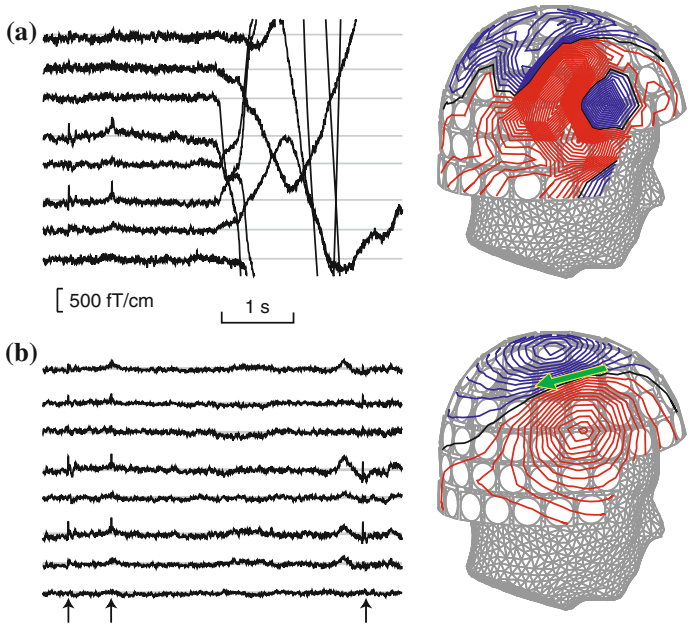

Fig. 8 An example of tSSS and movement correction. **a** *Left*: Five seconds of original raw data on six gradiometer channels above the right somatosensory cortex. The head began continuous movement approximately 3 s after the beginning of the data traces and the added magnetized piece above the somatosensory cortex emanated a very strong artifact. *Right*: The spatial MEG pattern at the N30m peak response from averaged somatosensory evoked fields (SEF). **b** The same raw data and MEG pattern after tSSS and head movement correction were employed. The *arrows* indicate single SEF responses

of the sensors. The tSSS method has been shown to work in a satisfactory manner against several different kinds of artifacts induced by magnetized pieces on the scalp (Taulu and Hari 2009), head movements (Nenonen et al. 2012), dental work (Hillebrand et al. 2013), and implanted stimulators such as DBS (Airaksinen et al. 2011) and VNS (Carrette et al. 2011; Kakisaka et al. 2012; Tanaka et al. 2009). A quite similar method utilizing reference sensors instead of SSS as the original separation method has been proposed by de Cheveigné and Simon (2007). An example of tSSS interference suppression is shown in Fig. 8 for disturbances caused by magnetized material on the scalp and head movement.

3.5.5 Feedback Active Compensation

In the feedback active compensation method, we use magnetometer sensors on the MEG helmet as null detectors in a negative feedback loop that controls currents in coils on the inside walls of the MSR. The magnetic fields from these coils counteract the ambient interference and keep the field constant at the locations of

the zero detectors. This helps keep the interference field within the dynamic range of the sensors in the entire MEG helmet. Interference rejection performance provided by this method is limited by geometry: the magnetic field is kept strictly constant at the location of the zero-detector magnetometers only. Because the counteracting field shapes obtained from the coils on the walls differ from the interference field shapes, it is not possible to exactly cancel the field in all MEG magnetometers distributed over the relatively large volume in the sensor helmet. Typically using six coils—a "Helmholz-pair" in all three principal directions of the MSR—an interference rejection ratio of about 10 can be achieved over the entire sensor array. A method to get around this geometric limitation in shielding performance and to achieve a higher shielding factor by this feedback active compensation has been described in a patent application (Simola and Taulu 2011).

An active compensation arranged in this way naturally distorts the spatial pattern of the biomagnetic signals. The method keeps also the biomagnetic signal at zero in the null-detector channels. The compensation coils, however, are simply sources of external interference and any method appropriately compensating for such interference also restores the unbiased brain signals in all sensors, including the zero-detector channels. In the present implementation of active compensation, the SSS method is used for this purpose.

3.5.6 Principal and Independent Component Analysis

Principal component analysis (PCA) decomposes data into orthogonal component vectors via a singular value decomposition of the covariance matrix. PCA is applied to compose the vectors spanning the interference subspace, typically from MEG data recorded in an empty magnetically shielded room as described in Sect. 3.5.2. PCA can also be applied to subject-based interference such as fields due to eye blinks and heartbeat. Data from a large enough number of such disturbances are extracted and few most prominent PCA vectors are selected to represent the subject interference, to be projected out from the MEG and EEG data after the recording.

Independent component analysis (ICA) is a newer technique which aims at separation of unknown sources whose unknown mixture is measured by the sensors:

$$\phi(t) = \mathbf{A}\mathbf{s}(t), \tag{21}$$

where $\phi(t)$ is the signal vector at time t, $\mathbf{s}(t)$ represents the instantaneous source activity, and matrix $\mathbf{A}$ represents the mixing. The ICA procedure provides an estimate of the unmixing matrix $\mathbf{B}$ so that the estimated source activity becomes

$$\hat{\mathbf{s}}(t) = \mathbf{B}\phi(t). \tag{22}$$

ICA belongs to the family of blind source separation methods, because the source signals are not directly observed and nothing is known about their mixture; the only

assumption is that the sources $\mathbf{s}(t)$ are statistically independent. The separation is obtained by optimizing a contrast function of some distributional property of the output $\hat{s}$. The contrast functions are based on entropy, mutual independence, high-order decorrelations, etc. (see, e.g., Cardoso 1998; Hyvärinen 1999).

ICA has been applied to MEG and EEG to mainly remove artifacts (e.g., Vigario et al. 2000). ICA has also been used to decompose MEG/EEG data into separate components (e.g., Tang et al. 2002). However, the underlying assumption of statistical independence between the activations of the different neural sources may not be valid for a physiologically plausible separation of distinct neural processes or sources. Nevertheless, applying ICA to a suitable sparsifying transformation of the MEG data may help extract relevant brain activity patterns (Hyvärinen et al. 2010; Ramkumar et al. 2012).

3.5.7 Sensor Noise Suppression

By sensor noise we mean random noise signals that are inherent to the MEG sensors and independent from other sensors. Such a noise component does not have a unique overall field pattern that could be modeled and subtracted from all sensors simultaneously. Therefore, the traditional way of addressing sensor noise is by statistical means, e.g., by estimating the noise covariance matrix of the sensors and taking it into account in source modeling.

Recently de Cheveigné and Simon (2008) proposed a sensor noise reduction approach that is based on the assumption that sensor noise is uncorrelated with brain activity and uncorrelated between sensors. In their method, PCA is applied iteratively by omitting one channel at a time. The data of the omitted channel is replaced by its regression on the subspace formed by the other channels. Computation time is saved by orthogonalizing a subset of channels selected on the basis of correlation with the omitted channel data. Even more recently, a similar approach has been proposed (Taulu et al. 2012) with the difference that the model for the spatially correlated part of the sensor signals is estimated with a physical model based on SSS instead of using statistics such as PCA. Both of the above methods decrease the random sensor noise significantly and improve the signal-to-noise ratio of the brain signals. The SSS based method was recently demonstrated to reduce the overall sensor noise level in the frequency band of 400–800 Hz by factors of 4.5 and 2.1 for gradiometers and magnetometers, respectively (Helle et al. 2012).

Denoising source separation, DSS (Särelä and Valpola 2005) is yet another way to suppress noise contributions from the sensors and background brain activity. DSS is an iterative method that refines a template filter, often seeded by ICA, applied on whitened data. The method has been demonstrated on single-trial MEG data (Karp et al. 2009). DSS was utilized also by de Cheveigné (2010) for constructing a spatiotemporal filter to partition the recorded data into signal and noise components. Time-shifted signals and PCA are utilized to construct special FIR filters, and averaged evoked responses are utilized as a contrast function to emphasize the brain activity.

3.5.8 Spatial Filtering Combined with Source Modeling

Spatial filtering methods, such as beamforming, aim at finding and characterizing the neural current sources in the brain (Vrba and Robinson 2001). A spatial filter is constructed so that it passes the activity at the target location with unit gain while suppressing the contribution from other sources. Spatial filtering can thus suppress unwanted interference, provided that the low-rank interference has spatially and temporally distinctly different characteristic from the brain signals (Sekihara et al. 2004). Typically such interference originates outside of the magnetically shielded room, but the beamformer technique has been demonstrated to successfully suppress nearby interference from a pain stimulator (Adjamian et al. 2009). However, the basic assumptions are not valid in cases where the patient-induced artifacts, e.g. due to dental braces, are huge compared to the brain signals (Hillebrand et al. 2013).

Another approach to combine source imaging and interference suppression was suggested by Mosher et al. (2009). They placed a grid of dipoles inside the MEG helmet and used their lead fields to compose the basis of the signal subspace. Its null space was then used to construct a blocking operator for removing all neural activity components from the measured data. Projection of unwanted interference waveforms is basically similar to the temporal SSS presented above, but the method can produce current source estimates for the analysis without a separate step.

3.5.9 Physiological Artifacts

While SSS can geometrically separate the brain from external interference sources by the concentric inner and outer spheres, the method does not suppress signals from physiological sources in the inner volume or the space between the spheres. Such physiological artifacts include signals from head muscles, eyes (blinks and saccades), or cardiac signals due to cardiac volume currents and pulsating blood flow within this intermediate space. If strong cardiac or eye-blink artifacts are present, a further post-processing to suppress them can be performed with the signal space projection method (Uusitalo and Ilmoniemi 1997). In this case, instead of applying PCA directly on the continuous signals, it is often beneficial to average with respect to these stereotypical artifacts to boost them relative to brain signals and then perform PCA on the average. Identification and suppression of the neck muscle artifacts could be performed utilizing methods such as independent component analysis (Vigario et al. 2000). Generally, individual variations exist between subjects with respect to the heartbeat-related residual after SSS.

4 Future Prospects

The adoption of modern signal processing methods to multi-channel MEG data has advanced the MEG interference suppression rapidly during the last few years. In addition, solely hardware-based magnetic shielding has shifted towards active

shielding methods, which are less expensive and lighter-weight than conventional passive means and thus allow more flexibility in planning the location of an MEG laboratory. These trends are likely to continue in the future to support wider adoption of MEG, not only through cost reduction but also by allowing MEG to be applied to patients with magnetic material in their body. In the following, we try to highlight some of the future opportunities and challenges of interference suppression in MEG.

4.1 MEG Without a Shielded Room

As an ultimate goal for interference suppression, one could envision an MEG system without a magnetically shielded room. Since the room constitutes roughly 20 % of the total cost of a MEG set-up, replacing the expensive passive shield altogether with an active system is tempting. However, operating an MEG system in a magnetically harsh, or even average, environment without any passive shielding is challenging for the following reasons: (i) the combination of the sensors, the active compensation system and the software-based interference suppression method should have a very large dynamic range (in excess of 140 dB) in order to cope with the largest interference signals while not elevating the sensor noise floor, (ii) the compensation system should be able to deal with the high-order field gradients due to near-by interference sources, (iii) Earth's static magnetic field (500–1,000 times stronger than the remanent field in a typical MSR) polarizes paramagnetic objects which cause additional interference when moving or vibrating within or in the vicinity of the sensor helmet, (iv) SQUIDs must be shielded against radio-frequency interference (see Sect. 1.4); a passive magnetically shielded room acts as an RF shield as well and thus a system without such a room may still require an RF-shield around it for reliable operation if the sensor elements cannot be RF-shielded locally. Despite these problems, proof-of-concept MEG measurements without a shielded room have been performed in magnetically quiet environments. However, reliable unshielded MEG operation in typical environments will become possible only after considerable advances regarding the above challenges.

4.2 Novel Sensor Technologies

Low-Tc SQUIDs have so far been the sensor of choice for serious MEG instrumentation due to their excellent noise performance and stability; however, these sensors require expensive liquid-helium cooling, and the large temperature gradient necessitates elaborate thermal insulation which introduces a considerable gap from the scalp to the sensors. New sensor technologies that may alleviate these problems have emerged recently. High-Tc SQUIDs (see the work by Öisjöen and

colleagues (2012) for a recent MEG application) and "mixed sensors" (Pannetier et al. 2004; Pannetier-Lecoeur et al. 2011) can be operated in liquid nitrogen, avoiding much of cryogenics-related costs, and brought closer to the scalp. Atomic magnetometers are based on optical detection of magnetic-field-induced light polarization changes in alkali-metal vapors; these sensor operate at +120 to +150 C and they can also be located within a few mm from the scalp. Atomic magnetometers allow a non-rigid sensor helmet that can be adapted to the head size and shape of individual subjects. Devices using liquid nitrogen may also allow some degree of geometric adaptability if the sensor array is split into multiple small dewars.

These considerable improvements in MEG instrumentation will have implications for interference suppression. Bringing the sensors closer to the scalp implies that higher spatial frequencies can be measured, which improves source reconstruction accuracy but also requires that the physics-based interference suppression methods, such as SSS, have to be adapted accordingly to work efficiently. On the other hand, an adaptable snugly-fitting sensor array is likely to deviate from a sphere more than the current fixed array, which makes the SSS transform numerically more stable and may provide a higher shielding factor. However, the adaptability of the array calls for very accurate yet quick means to determine the locations and orientations of the sensors in order to efficiently use these physics-based methods for decomposing the data to neural signals and interference. On the contrary, statistics-based adaptive methods, such as SSP, would not need the geometric information but would lack the generic nature of SSS.

4.3 Hybrid Instrumentation

Very recently, large-scale MEG has been successfully combined with ultra-low-field (ULF) MRI in the same system (Vesanen et al. 2012). This combination is attractive since the SQUID sensor array can be efficiently used for both MEG and ULF-MRI signal acquisition. However, for a decent signal-to-noise ratio in ULF-MRI, the low measurement field ($\sim$100 μT) has to be accompanied with a stronger pre-polarization field (typically 10–100 mT) that is switched on briefly before collecting the data. The SQUID sensors should be highly resistant to flux traps so that they can recover within few milliseconds from the pre-polarization field. Such field tolerance of the sensors would be beneficial also for MEG when operating the system in a very light shield or completely without a shielded room.

Similarly to MEG, the MRI mode of the hybrid MEG–MRI system benefits from efficient interference suppression. Although the MRI signals are in the kHz range where environmental interference is usually not of concern, reduction of the intrinsic sensor noise, as outlined in Sect. 3.5.7, could considerably improve image quality. In addition, noise of the MRI gradient amplifiers may propagate to the sensors via the gradient coils. Since the field pattern of such interference is constant, projection methods such as SSP should work efficiently.

5 Conclusion

The MEG measurement technology has taken huge steps forward since the early days when the number of recording channels was one or only a few. Novel interference and noise suppression methods have emerged as a kind of byproduct of the significant increase in the number of recording channels. Because at present the number of detectable degrees of freedom in the magnetic brain signal is known to be around 80 only, modern devices containing over 300 independent channels oversample the actual neuromagnetic field. This fact has enabled efficient general-purpose interference and noise reduction methods such as signal space projection (SSP) and signal space separation (SSS).

Because interfering magnetic fields—even when MEG is performed in a magnetically shielded room—may exceed the strength of the neuromagnetic signal by about a factor of thousand, it is actually necessary to record the interference with a better relative accuracy than the neuromagnetic signal itself; Only this enables sufficiently precise subtraction of the interference from the recorded raw signal. To achieve such an accuracy, it is necessary to use the entire set of MEG channels for this purpose, not only a limited set of reference channels as was done in the early 1990s. Thanks to the ample oversampling of the magnetic field, signal space methods can then be used to determine and subtract the interference signal from the recorded raw signal.

With the help of such effective "software magnetic shielding" the required hardware shielding, magnetically shielded room, can be made lighter and cheaper. This may be an effective booster for the adoption of MEG in hospitals.

References

Adjamian P, Worthen S, Hillebrand A, Furlong P, Chizh B, Hobson A, Aziz Q, Barnes G (2009) Effective electromagnetic noise cancellation with beamformers and synthetic gradiometry in shielded and partly shielded environments. J Neurosci Methods 178(1):120–127

Ahonen A, Hämäläinen M, Ilmoniemi R, Kajola M, Knuutila J, Simola J, Vilkman V (1993) Sampling theory for neuromagnetic detector arrays. IEEE Trans Biomed Eng 40:859–869

Airaksinen K, Mäkelä J, Taulu S, Ahonen A, Nurminen J, Schnitzler A, Pekkonen E (2011) Effects of DBS on auditory and somatosensory processing in Parkinson's disease. Hum Brain Mapp 32(7):1091–1099

Arfken G (1985) Mathematical methods for physicists. Academic Press, San Diego

Bork J, Hahlbohm HD, Klein R, Schnabel, A (2001) The 8-layered magnetically shielded room of the PTB: design and construction. In: Biomag2000, Proceedings of the 12th international conference on biomagnetism, Helsinki University of Technology, Espoo, Finland 2000, p 970–973

Cardoso J (1998) Blind signal separation: statistical principles. Proc IEEE 86:2009–2025

Carrette E, De Tiège X, Op De Beeck M, De Herdt V, Meurs A, Legros B, Raedt R, Deblaere K, Van Roost D, Bourguignon M, Goldman S, Boon P, Van Bogaert P, Vonck K (2011) Magnetoencephalography in epilepsy patients carrying a vagus nerve stimulator. Epilepsy Res 93(1):44–52

Chella F, Zappasodi F, Marzetti L, Della Penna S, Pizzella V (2012) Calibration of a multichannel MEG system based on the signal space separation method. Phys Med Biol 57(15):4855–4870

Clarke J, Braginski A (eds) (2006) The SQUID handbook. Wiley-VCH, Weinham

Cohen D (1968) Magnetoencephalography: evidence of magnetic fields produced by alpha-rhythm current. Science 161:784–786

Cohen D (1970) Large-volume conventional magnetic shields. Rev Phys Appl 5:53–58

Cohen D (1972) Magnetoencephalography: detection of the brain's electrical activity with a superconducting magnetometer. Science 175:664–666

Cohen D (1979) Magnetic measurement and display of current generators in the brain. Part I: the 2-d detector. In: Proceedings of the 12th international conference on medical and biological engineering, Jerusalem, pp 15–16

De Cheveigné A, Simon J (2007) Denoising based on time-shift PCA. J Neurosci Methods 165:297–305

De Cheveigné A, Simon J (2008) Sensor noise suppression. J Neurosci Methods 168(1):195–202

De Cheveigné A (2010) Time-shift denoising source separation. J Neurosci Methods 189(1):113–120

De Tiège X, Op de Beeck M, Funke M, Legros B, Parkkonen L, Goldman S, Van Bogaert P (2008) Recording epileptic activity with MEG in a light-weight magnetic shield. Epilepsy Res 82(2–3):227–231

Gross J, Baillet S, Barnes G, Henson R, Hillebrand A, Jensen O, Jerbi K, Litvak V, Maess B, Oostenveld R, Parkkonen L, Taylor J, van Wassenhove V, Wibral M, Schoffelen J (2013) Good practice for conducting and reporting MEG research. Neuroimage 65:349–363

Hall Barbosa C, Andrade Lima E, Bruno A, Ewing A, Wikswo JP Jr (1999) Flux/voltage calibration of axial SQUID gradiometers using an optimization procedure. IEEE Trans App Supercond 9:3523–3526

Hämäläinen M, Hari R, Ilmoniemi RJ, Knuutila J, Lounasmaa OV (1993) Magnetoencephalography—theory, instrumentation, and applications to noninvasive studies of the working human brain. Rev Mod Phys 65:413–498

Helle L, Parkkonen L, Taulu S. Ahonen A (2012) Suppression of uncorrelated sensor noise and artifacts: demonstration with high frequency brain signals. Abstracts of the 18th international conference on biomagnetism, Paris 2012, p 284

von Helmholtz H (1853) Ueber einige Gesetze der Vertheilung elektrischer Ströme in körperlichen Leitern, mit Anwendung auf die thierisch-elektrischen Versuche. Ann Phys Chem 89(211–233):353–377

Hill E (1954) The theory of vector spherical harmonics. Am J Phys 22:211–214

Hillebrand A, Pazio P, de Munck J, van Dijk B (2013) Feasibility of clinical magnetoencephalography (MEG) functional mapping in the presence of dental artefacts. Clin Neurophysiol 124(1):107–113

Hyvärinen A (1999) Fast and robust fixed-point algorithms for independent component analysis. IEEE Trans Neural Netw 10:626–634

Hyvärinen A, Ramkumar P, Parkkonen L, Hari R (2010) Independent component analysis of short-time Fourier transforms for spontaneous EEG/MEG analysis. Neuroimage 49:257–271

Ilmoniemi R (1981) 7-channel SQUID magnetometer for brain research. M.Sc. thesis, Helsinki University of Technology

Ilmoniemi R, Williamson S (1987) Analysis of the magnetic alpha rhythm in signal space. Soc Neurosci Abstr 13:46

Ilmoniemi R, Williamson S, Hostetler W (1987) New method for the study of spontaneous brain activity. Biomagnetism 87. Tokyo Denki University Press, Tokyo, p 182–185

Jackson J (1999) Classical electrodynamics. John Wiley & Sons, Inc, New York

Kakisaka Y, Mosher J, Wang Z, Jin K, Dubarry A, Alexopoulos A, Burgess R (2012) Utility of temporally-extended signal space separation algorithm for magnetic noise from vagal nerve stimulators. Clin Neurophysiol

Karp E, Parkkonen L, Vigário R (2009) Denoising single trial event related magnetoencephalographic recordings. In: Adali T et al (eds) Independent component analysis and signal separation, Springer, Berlin, pp 427–434

Kelhä V, Pukki J, Peltonen R, Penttinen A, Ilmoniemi R, Heino J (1982) Design, construction, and performance of a large-volume magnetic shield. IEEE Trans Magn MAG-18:260–270

Kiviranta M, Seppä H (1995) DC-SQUID electronics based on the noise cancellation scheme. IEEE Trans Appl Superconduct 5(2):2146–2148

Kominis I, Kornack T, Allred J, Romalis M (2003) A subfemtotesla multichannel atomic magnetometer. Nat London 422:596

Mosher J, Hämäläinen M, Pantazis D, Hui H, Burgess R, Leahy R (2009) Generalized sidelobe canceller for magnetoencephalography arrays. Proc IEEE Int Symp Biomed Imaging. 2009:149–152

Nenonen J, Montonen J, Katila T (1996) Thermal noise in biomagnetic measurements. Rev Sci Instr 67(6):2397–2405

Nenonen J, Kajola M, Simola J, Ahonen A (2004) Total information of multichannel MEG sensor arrays. Proceedings of the 14th international conference on biomagnetism, Biomag Ltd., Boston 2004, p 630–631

Nenonen J, Taulu S, Kajola M, Ahonen A (2007) Total information extracted from MEG measurements. Int Congr Ser 1300:245–248

Nenonen J, Nurminen J, Kičić′ D, Bikmullina R, Lioumis P, Jousmäki V, Taulu S, Parkkonen L, Putaala M, Kähkönen S (2012) Validation of head movement correction and spatiotemporal signal space separation in magnetoencephalography. Clin Neurophysiol 123(11):2180–2191

Nurminen J, Taulu S, Okada Y (2008) Effects of sensor calibration, balancing and parametrization on the signal space separation method. Phys Med Biol 53(7):1975–1987

Ornelas P, Bruno A, Hall Barbosa C, Andrade Lima E, Costa Ribeiro P (2003) A survey of calibration procedures for SQUID gradiometers. Supercond Sci Technol 16:427–431

Pannetier M, Fermon C, Goff G, Simola J, Kerr E (2004) Femtotesla magnetic field measurement with magnetoresistive sensors. Science 304:1648–1650

Pannetier-Lecoeur M, Parkkonen L, Sergeeva-Chollet N, Polovy H, Fermon C, Fowley C (2011) Magnetocardiography with sensors based on giant magnetoresistance. Appl Phys Lett 98:153705

Parkkonen L, Simola J, Tuoriniemi J, Ahonen A (1999a) An interference suppression system for multichannel magnetic field detector arrays. In: Yoshimoto T et al (eds) Recent advances in biomagnetism: proceedings of the 11th international conference on biomagnetism, pp 13–16, Tohoku University Press

Parkkonen L, Simola J, Kajola M, Hämäläinen M, Ahonen A (1999b) Experiments on interference suppression in MEG measurements. Abstracts of the human brain mapping conference, Düsseldorf 1999, #165

Parkkonen L, Simola J, Taulu S, Kajola M, Knuutila J, Kojo A, Laine P, Nenonen J, Ahonen A (2006) A light-weight magnetic shield: performance in real MEG measurements. Proceedings of the 15th International Conference on Biomagnetism, Vancouver, BC, Canada, 21–25 Aug 2006. Abstracts of the 15th International Conference on Biomagnetism, Vancouver 2006

Parkkonen L, Salmelin R (2010) Ch3: Measurements. In: Hansen P, Kringelbach M, Salmelin R (eds) MEG: an introduction to methods, Oxford University Press, New York

Patton B, Fitch J (1962) Design of a room-size magnetic shield. J Geophys Res 67(3):1117

Ramirez R, Kopell B, Butson C, Hiner B, Baillet S (2011) Spectral signal space projection algorithm for frequency domain MEG and EEG denoising, whitening, and source imaging. Neuroimage 56(1):29–78

Ramkumar P, Parkkonen L, Hari R, Hyvärinen A (2012) Characterization of neuromagnetic brain rhythms over time scales of minutes using spatial independent component analysis. Hum Brain Mapp 33:1648–1662

Särelä J, Valpola H (2005) Denoising source separation. J Mach Learn Res 6:233–327

Sekihara K, Nagarajan S, Poeppel D, Marantz A (2004) Performance of an MEG adaptive-beamformer source reconstruction technique in the presence of additive low-rank interference. IEEE Trans Biomed Eng 51(1):90–99
Simola J (2003) Wall element for magnetically shielded room and magnetically shielded room. Patent WO/2003/059030
Simola J, Laine P, Rakkolainen H (2005) Joint structure between the wall elements of a magnetically shielded room, PCT/FI05/00385
Simola J, Taulu S (2011) Method for designing coil systems for generation of magnetic fields of desired geometry, PCT/FI2011/050249
Tanaka N, Thiele E, Madsen J, Bourgeois B, Stufflebeam S (2009) Magnetoencephalographic analysis in patients with vagus nerve stimulator. Pediatr Neurol 41(5):383–387
Tang A, Pearlmutter B, Malaszenko N, Phung D, Reeb B (2002) Independent components of magnetoencephalography: localixation. Neural Comput 14:1827–1858
Taulu S (2000) M.Sc. thesis (in Finnish), Helsinki University of Technology
Taulu S, Kajola M, Simola J (2004) Suppression of interference and artifacts by the signal space separation method. Brain Topogr 16(4):269–275
Taulu S, Kajola M (2005) Presentation of electromagnetic multichannel data: the signal space separation method. J Appl Phys 97(124905):1–10
Taulu S, Simola J, Kajola M (2005) Applications of the signal space separation method. IEEE Trans Sign Proc 53:3359–3372
Taulu S, Simola J (2006) Spatiotemporal signal space separation method for rejecting nearby interference in MEG measurements. Phys Med Biol 51(7):1759–1768
Taulu S (2008) Processing of weak magnetic multichannel signals: the signal space separation method. PhD Dissertation, Helsinki University of Technology
Taulu S, Hari R (2009) Removal of magnetoencephalographic artifacts with temporal signal-space separation: demonstration with single-trial auditory-evoked responses. Hum Brain Mapp 30(5):1524–1534
Taulu S, Simola J, Kajola M, Helle L, Ahonen A, Sarvas J (2012) Suppression of uncorrelated sensor noise and artifacts in multichannel MEG data. Abstracts of the 18th international conference on biomagnetism, Paris 2012, p 285
Uusitalo M, Ilmoniemi R (1997) Signal-space projection method for separating MEG or EEG into components. Med Biol Eng Comput 35(2):135–140
Vesanen P, Nieminen J, Zevenhoven K, Dabek J, Parkkonen L, Zhdanov A, Luomahaara J, Hassel J, Penttilä J, Simola J, Ahonen A, Mäkelä J, Ilmoniemi R (2012) Hybrid ultra-low-field MRI and magnetoencephalography system based on a commercial whole-head neuromagnetometer. Magn Reson Med (2012 Jul 17, epub ahead of print)
Vigario R, Särelä J, Jousmäki V, Hämäläinen M, Oja E (2000) Independent component approach to the analysis of EEG and MEG recordings. IEEE Trans Biomed Eng 47:589–593
Wikswo J (2004) SQUIDs remain best tools for measuring brain's magnetic field. Phys Today 57(2):15
Vrba J, Robinson S (2001) Signal processing in magnetoencephalography. Methods 25:249–271
Vrba J, Robinson S (2002) SQUID sensor array configurations for magnetoencephalography applications. Supercond Sci Technol 15:R51–R89
Vrba J, Taulu S, Nenonen J, Ahonen A (2010) Signal space separation beamformer. Brain Topogr 23(2):128–133
Zimmerman J, Frederick N (1971) Miniature ultrasensitive superconducting magnetic gradiometer and its use in cardiography and other applications. Appl Phys Lett 19:16
Öisjöen F, Schneiderman J, Figueras G, Chukharkin M, Kalabukhov A, Hedström A, Elam M, Winkler D (2012) High-Tc superconducting quantum interference device recordings of spontaneous brain activity: towards high-Tc magnetoencephalography. Appl Phys Lett 100:132601

http://www.springer.com/978-3-642-33044-5

Magnetoencephalography
From Signals to Dynamic Cortical Networks
Supek, S.; Aine, C.J. (Eds.)
2014, XXI, 1013 p. 266 illus., 215 illus. in color.,
Hardcover
ISBN: 978-3-642-33044-5